The CEPR2-mediated phosphorylation of NRT1.2 mainly regulates ABA import in *Arabidopsis*

Zipeng Yu [1, δ], Lei Zhang [1, δ], Yang Xu [1], Miao Yu [2], Shizhong Zhang [1], Guodong Yang [1], Jinguang Huang [1], Kang Yan [1], Chengchao Zheng [1, *] and Changai Wu [1, *]

[δ] These authors contributed equally to this work.

[1] State Key Laboratory of Crop Biology, Shandong Agricultural University, Tai'an 271018, China

[2] State Key Laboratory of Plant Physiology and Biochemistry, College of Biological Sciences, China Agricultural University, Beijing 100193, China

* **Corresponding authors**

Chengchao Zheng: cczheng@sdau.edu.cn; Tel: 86-538-8242894

Changai Wu: cawu@sdau.edu.cn; Tel: 86-538-8246858

E-mails:

Zipeng Yu: yzp52120090916@163.com

Lei Zhang: zhanganqi2002@163.com

Yang Xu: xy52120092661@163.com

Miao Yu: ym15600911706@126.com

Shizhong Zhang: shizhong@sdau.edu.cn

Guodong Yang: gdyang@sdau.edu.cn

Jinguang Huang: jghuang@sdau.edu.cn

Kang Yan: kangyan@sdau.edu.cn

Chengchao Zheng: cczheng@sdau.edu.cn

Changai Wu: cawu@sdau.edu.cn

Abstract

ABA signaling and transport play important roles in plant systematic responses to environmental factors. Previously, we reported that C-terminally encoded peptide receptor 2 (CEPR2) balances plant growth and ABA responses by phosphorylating abscisic acid (ABA) receptors. Here, we showed that CEPR2 also directly phosphorylated the ABA transporter NRT1.2 by phosphaproteomics analysis using CEPR2 overexpression line and by physiological and biochemical experiments. Using transgenic seedlings, we demonstrated that NRT1.2 positively regulated the ABA response, and that CEPR2 acted on NRT1.2 epistatically. Specifically, CEPR2 phosphorylated NRT1.2 at serine 292 (Ser^{292}) to promote the degradation of NRT1.2 via the 26S proteasome and vacuolar degradation pathways. However, ABA strongly inhibited the phosphorylation of NRT1.2 at Ser^{292}, stabilizing NRT1.2. Transportation assays in yeast and *Xenopus* oocytes showed that the nonphosphorylation of NRT1.2 showed high ABA but very low nitrate import activity, while the phosphorylation of NRT1.2 by CEPR2 eliminated NRT1.2-mediated ABA import but slightly increased nitrate transport. These findings were consistent with our analyses of complement mutants *in planta*. Thus, our results provide detailed mechanisms of NRT1.2 in transporting ABA and nitrate in response to environmental conditions in plants. Besides, it is a better way for plants to overexpress the unphosphorylated NRT1.2 at Ser^{292} both under high and low nitrate conditions.

Keywords

ABA; CEPR2; NRT1.2; Phosphorylation; Degradation; Transporter activity

Introduction

Plants must continuously adapt to adverse environmental conditions, including temperature, salinity, nitrate (NO_3^-), or drought (Li et al., 2019; Soma et al., 2017; Teardo et

al., 2019; Xu et al., 2018; Yang et al., 2019; Zhang et al., 2018). Upon sensing environmental stressors, plants stop growing and trigger protective responses (Wang et al., 2018). Once environmental stresses subside, plants quickly deactivate protective responses and reinitiate growth (Wang et al., 2018). The mechanisms that regulate the switch between growth and stress responses are critical for plant survival, but still not fully elucidated.

Abscisic acid (ABA), a stress hormone, is critical in the regulation of a wide range of stress responses and plant growth (Cutler et al., 2010; Raghavendra et al., 2010). In response to environmental stress, ABA accumulates rapidly and is transported from the site of synthesis to the site of action, where it is recognized by ABA receptors in the pyrabactin resistance 1 family (PYR1); these proteins are also referred to as PYR1-like (PYL) (Boursiac et al., 2013). C-terminally encoded peptide receptor 2 (CEPR2), which is a typical leucine-rich repeat receptor-like kinase (LRR-RLK), controls the interaction between plant growth and the stress response in *Arabidopsis* by regulating the phosphorylation and degradation of ABA-receptor PYLs in response to environmental conditions (Yu et al., 2019). However, the mechanisms in CEPR2-mediated ABA response need further investigation.

ABA is predominantly produced in vascular tissues in response to drought stress (Boursiac et al., 2013). ABA transporters play key roles in the long-distance transport of ABA through the plasma membrane (PM) to the active site. As reviewed by Kuromori (ABA transporter and plant water stress), several ABA transporters have been identified (Kuromori et al., 2010). Two Arabidopsis AT-binding cassette (ABC) transporters, AtABCG25 and AtABCG40, have been identified as ABA transporters involved in the ABA sensitivity or stomatal closure based on the phenotypes of mutants defective in the respective proteins (Kang et al., 2015; Kuromori et al., 2010). Biochemical characterization using heterologous expression systems has shown that AtABCG25 and AtABCG40 exhibit ABA export and import activity, respectively (Kang et al., 2015; Kuromori et al., 2010). Functional screening

using a yeast system identified an Arabidopsis NITRATE TRANSPORTER 1/PEPTIDE TRANSPORTER FAMILY (NPF) member, NPF4.6 (originally named AIT1), as a protein that could mediate ABA uptake into cells (Kanno et al., 2012). NPF4.6 was previously characterized as a low-affinity nitrate transporter NRT1.2. Besides, a member of the multidrug and toxin efflux (MATE) transporter family, AtDTX50, has also been identified as an ABA exporter (Zhang et al., 2014). However, the transporting mechanisms of ABA transporters remain largely unknown.

Here, we showed that in the absence of ABA, CEPR2 phosphorylates NRT1.2 at Ser^{292} to promote its degradation. This phosphorylation completely inhibited the NRT1.2-mediated ABA but slightly increased the nitrate importing. However, ABA strongly inhibited the phosphorylation at Ser^{292} and the degradation of NRT1.2, leading to the resumption of ABA-import functionality. Therefore, CEPR2 regulates the ABA response also by interacting with the ABA transporter. Our results provide valuable regulatory mechanisms underlying ABA transporter activity and information for plant biotechnological breeding.

Results

The loop region of NRT1.2 interacted with the kinase domain of CEPR2

To investigate the regulatory mechanisms underlying the response of CEPR2 to ABA, we compared the phosphoproteomes of wild-type (WT) *Arabidopsis* seedlings to those of CEPR2-OE-9, a previously described *Arabidopsis* line overexpressing CEPR2 (Yu et al., 2019). We identified 169 differentially expressed phosphopeptides ($p \leq 0.05$ and fold-change ≥ 1.20 or ≤ 0.8), of which 97 (belong to 78 proteins) were upregulated and 72 (belong to 68 proteins) were downregulated (Supplementary Excel 1). To identify the directly-phosphorylated target proteins of CEPR2, we examined the 78 upregulated proteins (Supplementary Table 1), and examined their interactions with CEPR2 using yeast two hybrid

(Y2H) experiments with the mating-based split ubiquitin system (MbSUS) (Supplementary Fig. 1b). Ten of the proteins were shown to interact with CEPR2 in the MbSUS assays (Supplementary Fig. 1b), including NRT1.2 (numbered as 46), which has previously been identified as an ABA and nitrate transporter (Huang et al., 1999; Kanno et al., 2012). We thus focused on NRT1.2 in subsequent experiments investigating the interaction mechanisms in the ABA signaling pathway.

To further confirm the interaction of NRT1.2 and CEPR2, firefly luciferase complementation imaging (LCI) assays were carried out. The results indicated that NRT1.2 interacted with CEPR2 *in vivo* (Fig. 1a). We then co-delivered the corresponding constructs of *CEPR2* and *NRT1.2* into tobacco epidermal leaf cells to perform bimolecular fluorescence complementation (BiFC) assays. Reconstituted YFP proteins and the plasma membrane (PM) marker N-(3-triethylammomiumpropyl) 4-(p-diethylaminophenylhexa-trienyl) (FM4-64) were co-localized on the PM (Fig. 1b). These data confirmed the interaction of NRT1.2 and CEPR2.

The differential phosphoproteome analysis showed that the phosphorylation sites are serine 277 and 292 residues (Ser^{277} and Ser^{292}) (Supplementary Excel 1). These two sites located in the cytosol loop region of NRT1.2 between two of the 12 transmembrane regions as shown in Fig. 1c. CEPR2 has a cytosol kinase domain as shown in Fig. 1c, too. Therefore, NRT1.2 might be phosphorylated by the kinase domain of CEPR2. To text this, we carried out MbSUS assay using the cytosol loop region of NRT1.2 ($NRT1.2^{loop}$) and series constructs used in the previous report (Yu et al., 2019). The results indicated that the $NRT1.2^{loop}$ interacted with the kinase domain of CEPR2 ($CEPR2^{KD}$) (Fig. 1d). Then we expressed recombinant $NRT1.2^{loop}$-GST and $CEPR2^{KD}$-His in *E. coli*. We used the purified GST proteins to perform pull down assays and found that $CEPR2^{KD}$ was pulled down by

NRT1.2^{loop}-GST but not by free GST (Fig. 1e). This further proved that the loop region of NRT1.2 interacted with the kinase domain of CEPR2.

Then we used MbSUS assays to investigate whether CEPR2 regulated other reported ABA transporters. The results showed that only the interaction between NRT1.2 and CEPR2 was detected (Fig. 1f). Moreover, we found no statistically significant differences in the transcription levels of genes encoding ABA transporters among CEPR2-OE-9, WT, and *cepr2-1* seedlings grown on 1/2 MS or 1 μM ABA medium (Supplementary Fig. 2). This suggested that CEPR2 did not affect the expression of genes encoding ABA transporters.

CEPR2 acts epistatically on NRT1.2

To determine how NRT1.2 participates in ABA signaling, we generated *Arabidopsis* plants overexpressing *NRT1.2* (*NRT1.2*-OE). *NRT1.2* transcription levels were much greater in the four *NRT1.2*-OE seedlings than in the WT seedlings (Fig. 2a). We also generated two T-DNA insertion mutants of *NRT1.2* (Fig. 2b) and found that *NRT1.2* gene expression levels in the *nrt1.2-1* seedlings (but not the *nrt1.2-2* seedlings) were much lower than that in the WT seedlings. However, NRT1.2 protein expression levels in both T-DNA seedlings (*nrt1.2-1* and *nrt1.2-2*) were obviously lower than that in the WT seedlings (Fig. 2c). The *NRT1.2*-OE, WT, *nrt1.2-1*, and *nrt1.2-2* seedlings were morphologically indistinguishable under normal conditions. However, when treated with ABA, the *NRT1.2*-OE seedlings grew slower than the WT seedlings, while the *nrt1.2-1* and *nrt1.2-2* seedlings grew faster (Fig. 2d). Accordingly, the *NRT1.2*-OE seedlings had shorter roots and exhibited slower seed germination rates as compared to the WT seedlings under ABA treatment, while the *nrt1.2-1* and *nrt1.2-2* seedlings had longer roots and faster seed germination rates (Fig. 2e, f). These results indicated that NRT1.2 enhanced ABA signaling. In contrast, a previous study indicated that CEPR2 inhibited ABA signaling(Yu et al., 2019), suggesting that CEPR2 might negatively regulate NRT1.2.

To further examine how CEPR2 and NRT1.2 expression affected ABA signaling, *cepr2-1* and *nrt1.2-1* plants were crossed. The *cepr2-1nrt1.2-1* plants showed similar degrees of ABA-insensitivity to the *nrt1.2-1* and *nrt1.2-2* plants; *cepr2-1nrt1.2-1* plants had longer roots and faster seed germination rates than the WT and *cepr2-1* seedlings after ABA treatment (Fig. 2d-f). This genetic evidence suggested that CEPR2 acts epistatically on NRT1.2 to affect ABA signaling.

CEPR2 reduced the stability of NRT1.2

The opposite response of *nrt1.2* and *cepr2* to ABA indicated that CEPR2 might affect NRT1.2 stability. To test this, cell-free degradation assays were carried out using the recombinant NRT1.2^{loop}-GST with protein extracts from CEPR2-OE-9, WT, and *cepr2-1* seedlings. Under normal conditions, NRT1.2^{loop}-GST was degraded more rapidly by protein extracts from CEPR2-OE-9 seedlings than by protein extracts from WT, while degraded similarly by protein extracts from *cepr2-1* and WT seedlings (Fig. 3a, b). In the presence of ABA, the NRT1.2^{loop}-GST degradation was significantly reduced by protein extracts from the *cepr2-1*, WT, and CEPR2-OE-9 seedlings (Fig. 3a, b). NRT1.2^{loop}-GST was degraded more rapidly by protein extracts from CEPR2-OE-9 seedlings than by protein extracts from WT, and in contrast by protein extracts from *cepr2-1* seedlings (Fig. 3a, b). These results suggested that CEPR2 accelerated the degradation of NRT1.2, but that this process was strongly inhibited by ABA.

To analyze the NRT1.2 degradation pathway, protein extracts from seven-day-old CEPR2-OE-9, WT, and *cepr2-1* seedlings were treated with 100 μM MG132 (an inhibitor of the 26S proteasome degradation pathway), 100 μM E64d (an inhibitor of the vacuolar degradation pathway), or both prior to incubation with purified NRT1.2^{loop}-GST. We found that NRT1.2 degradation was significantly suppressed by treatment with E64d and/or MG132, as compared to treatment with dimethyl sulfoxide (DMSO, the control; Fig. 3c). Specifically,

when NRT1.2^{loop}-GST fusion protein was decreased to 11% of initial levels after 2 h of treatment with DMSO when treated with protein extracts from CEPR2-OE-9 seedlings. Conversely, in protein extracts from CEPR2-OE-9 seedlings treated with MG132 or E64d for 2 h, NRT1.2^{loop}-GST fusion protein remained at 54% and 80% of initial levels, respectively (Fig. 3c). This suggested that NRT1.2 degradation was partially mediated by the 26S proteasome pathway and strongly mediated by the vacuolar degradation pathway. Consistent with this finding, NRT1.2^{loop}-GST fusion protein degradation by protein extracts from CEPR2-OE-9 seedlings was almost completely suppressed by treatment with a combination of E64d and MG132 (Fig. 3c). These results indicated that CEPR2 causes NRT1.2 degradation through the 26S proteasome and vacuolar degradation pathways.

CEPR2 reduced NRT1.2 stability dependent on the phosphorylation of the Ser^{292} residue of NRT1.2

Phosphorylation modifications regulate protein activity, stability, or interactions, and play a vital role in signal transduction (Chen et al., 2018). Our results above indicated that the phosphorylation of NRT1.2^{loop} was higher in CEPR2-OE-9 seedlings than in WT seedlings (Supplementary Excel 1), NRT1.2^{loop} interacted with CEPR2^{KD} (Fig. 1e) and CEPR2 accelerated NRT1.2 degradation (Fig. 3). Therefore, the effects of CEPR2 on NRT1.2 stability might depend on the phosphorylation states of Ser^{277} and/or Ser^{292}. To test this hypothesis, we performed *in vitro* kinase assays with the optimized NRT1.2^{loop} (Supplementary Fig. 3, 4) and found that when CEPR2^{KD}-His was incubated with NRT1.2^{loop}-GST in kinase buffer, the phosphorylation of NRT1.2^{loop}-GST increased (Fig. 4a). We then confirmed that CEPR2^{KD} interacted with mutated forms of NRT1.2 at Ser^{277} and/or Ser^{292} to the similarly sized, non-phosphorylatable, neutral alanine (A) and sustainably phosphorylatable, polar aspartate (D) and referred as NRT1.2^{loopS277A}, NRT1.2^{loopS292A}, NRT1.2^{loopS277D}, NRT1.2^{loopS292D}, NRT1.2^{loopS277AS292A}, and NRT1.2^{loopS277DS292D} (Supplementary Fig. 5). Subsequent *in vitro*

kinase assays showed that the phosphorylation level of NRT1.2^{loopS277A}-GST was similar to that of NRT1.2^{loop}-GST, but the mutation of NRT1.2^{loopS292A}-GST completely inhibited the phosphorylation (Fig. 4a). This indicated that the Ser^{292} residue of NRT1.2 is the primary site of CEPR2 phosphorylation.

Then we used cell free assays to determine whether ABA affects the phosphorylation of NRT1.2^{loop}. When purified recombinant NRT1.2^{loop}-GST was incubated with the protein extracts from CEPR2-OE-9 seedlings under control conditions (DMSO treatment, MG132 and E64d were used to block NRT1.2 degradation), phosphorylation levels gradually increased (Fig. 4b). However, phosphorylation levels were very low after purified recombinant NRT1.2^{loop}-GST was incubated with CEPR2-OE-9 protein extracts for up to 2 h in the presence of ABA (Fig. 4b). This indicated that ABA inhibited CEPR2-mediated NRT1.2 phosphorylation. Furthermore, compared with NRT1.2^{loop}, the degradation of NRT1.2^{loopS292A} was significantly inhibited irrespective of ABA treatment (Fig. 4c), suggesting that the phosphorylation of NRT1.2 at Ser^{292} is a prerequisite for CEPR2-mediated NRT1.2 degradation.

NRT1.2 phosphorylation eliminated NRT1.2-mediated ABA import

Then what are the effects of NRT1.2 phosphorylation on its ABA import activity. Since it has been reported that Y2H assays can be used to detect the interaction of PYLs with PP2C-type protein phosphatases in the presence of ABA (Kanno et al., 2012), we used Y2H assays to detect NRT1.2-mediated ABA import. In this experiment, ABI1 was fused to the GAL4 activation domain (AD-ABI1), and PYR1 fused to the GAL4 DNA-binding domain (BD-PYR1). The two constructs were co-transformed into yeast cells. Because the interaction of ABI1 and PYR1 dependent on the ABA level in yeast cells, so only when there contained ABA in yeast cells, can they grow well. The results showed that yeast cells with ‘AD-ABI1, BD-PYR1, and pYES2-NRT1.2’ grew faster than that yeast cells with ‘AD-ABI1, BD-PYR1,

and pYES2' after cultured in the -WLUAH medium containing 1 μM ABA (Fig. 5a, b), indicating that NRT1.2 stimulates ABA-import activity in yeast cells. However, no obvious growth differences between yeast cells after cultured in the -WLUAH medium containing 4 μM ABA (Supplementary Fig. 6). So -WLUAH medium containing 1 μM ABA was used for further analysis.

When grown in 1 μM ABA-supplemented -WLUAH media, yeast cells transformed with both CEPR2 and NRT1.2 grew significantly slower than those transformed with NRT1.2 only (Fig. 5a, b). Furthermore, pYES2-NRT1.2 vectors with nonphospho- and phospho-mimic forms at Ser277 and/or Ser292 (pYES2-NRT1.2^{S277A}, pYES2-NRT1.2^{S292A}, pYES2-NRT1.2^{S277AS292A}, pYES2-NRT1.2^{S277D}, pYES2-NRT1.2^{S292D}, and pYES2-NRT1.2^{S277DS292D}) were constructed and transformed into yeast cells containing AD-ABI1 and BD-PYR1 constructs. The transformed yeast cells with pYES2-NRT1.2^{S277A}, pYES2-NRT1.2^{S292A}, pYES2-NRT1.2^{S277AS292A}, or pYES2-NRT1.2^{S277D} constructs showed similar growth rate as the control, while yeast cells transformed with pYES2-NRT1.2^{S292D} or pYES2-NRT1.2^{S277DS292D} showed obviously lower growth than the control (Fig. 5a, b). These results suggested that only non-phosphorylated NRT1.2 at Ser^{292} is able to import ABA in yeast cells.

To further test the effects of CEPR2 phosphorylation on NRT1.2-mediated ABA import, we compared the levels of ABA transport activity in *Xenopus* oocytes in terms of ABA content. When *Xenopus* oocytes injected with NRT1.2 and nonphosphomimic-NRT1.2 (NRT1.2^{S292A}), we found significantly higher levels of ABA in *Xenopus* oocytes expressing NRT1.2 and NRT1.2^{S292A} as compared to negative control oocytes (injected with water; Fig. 5c), indicating that NRT1.2 also plays a role in ABA import in *Xenopus* oocytes. When *Xenopus* oocytes injected with phosphomimic-NRT1.2 (NRT1.2^{S292D}), no significant difference of ABA contents was detected compared with the negative control (Fig. 5c), further

demonstrating that phosphorylation at the Ser^{292} residue completely inhibited import of ABA by NRT1.2. *Xenopus* cells co-transformed with NRT1.2 and $CEPR2^{KD}$ contained similar levels of ABA as *Xenopus* cells expressing $NRT1.2^{S292D}$ (Fig. 5c). This indicated that it was the CEPR2-mediated phosphorylation of NRT1.2 that inhibited the import of ABA in *Xenopus* cells.

The effects of NRT1.2 phosphorylation on ABA-importing activities were further verified *in planta*. Both normal NRT1.2 and mutant $NRT1.2^{S292A}$ were introduced into *nrt1.2*-1 mutant to obtain complementary plants which were named as NRT1.2-COMs and $NRT1.2^{S292A}$-COMs (Supplementary Fig. 7). NRT1.2 complemented seedlings rescued the ABA-insensitive phenotype of *nrt1.2-1*, whereas $NRT1.2^{S292A}$ complemented seedlings had similar root length to those of NRT1.2-OE-1 (Fig. 5d). When exposed to ABA, both $NRT1.2^{S292A}$-COM and NRT1.2-OE-1 seedlings had shorter root length than WT seedlings and NRT1.2-COM seedlings (Fig. 5d). Consistent with this, ABA concentrations in $NRT1.2^{S292A}$-COM and NRT1.2-OE-1 seedlings were higher than that in the WT (Fig. 5e). NRT1.2 protein level in $NRT1.2^{S292A}$-COM seedlings was significantly higher than that in NRT1.2-COM seedlings (Fig. 5f), but there was no significant difference in *NRT1.2* transcription level (Supplementary Fig. 7). These results indicated that non-phosphorylated NRT1.2 was more stable than phosphorylated NRT1.2, and that non-phosphorylated NRT1.2 effectively imported ABA *in planta*.

Phosphorylated NRT1.2 slightly enhances nitrate transport activity

We found that Ser^{292} phosphorylation also affected the nitrate-transportation of NRT1.2 in *Xenopus* oocytes. NO_3^- concentrations in *Xenopus* oocytes expressing $NRT1.2^{S292D}$ were up to 11.6% higher NO_3^- content than in oocytes expressing NRT1.2 or $NRT1.2^{S292A}$ (Fig. 6a). This suggested that the phosphorylated NRT1.2 at Ser^{292} slightly enhanced NRT1.2-mediated NO_3^- import into *Xenopus* oocytes. Furthermore, we found that $NRT1.2^{S292A}$-COM-8

seedlings had slightly higher content of NO_3^- than NRT1.2-OE-1 seedlings, then NRT1.2-COM-2, WT, and *nrt1.2-1*seedlings at 3 h nitrate treatment (Fig. 6b). This suggested that NRT1.2 had low NO_3^- transport activity *in planta*. Consistently, NRT1.2^{S292A}-COMs and NRT1.2-OE seedlings had longer primary root length and higher fresh weight than NRT1.2-COM-1, WT, and *nrt1.2-1* seedlings under both low and high nitrate conditions (Fig. 6c-e). NRT1.2^{S292A}-COM seedlings showed similar phenotype with NRT1.2-OE seedlings (Fig. 6c-e), indicating the more stability of NRT1.2^{S292A} than the natural NRT1.2.

Discussion

ABA was a better substrate for NRT1.2 than NO_3^-

Although ABA and NO_3^- might theoretically compete substrates of NRT1.2, a previous study showed that high NO_3^- concentrations (100 mM) did not affect the ABA-importing activity of NRT1.2 (Kanno et al., 2013). Consistent with this, our results indicated that ABA was a better substrate for NRT1.2 than NO_3^-. First, both gain-of-function and loss-of-function approaches showed that NRT1.2 significantly affected plant root growth when exposed to ABA (Fig. 2d, e). However, there were no phenotypic differences among seedlings of *nrt1.2-1* and WT when exposed to high or low concentrations of nitrate (Fig. 6c-e). Second, NRT1.2 phosphorylation completely inhibited NRT1.2-mediated ABA import (Fig. 5a-c), but slightly increased NRT1.2-mediated NO_3^- transport in *Xenopus* oocytes (Fig. 6a). Third, NRT1.2 has been identified as a low-affinity nitrate transporter in *Xenopus* oocytes (Huang et al., 1999). Our results showed that although NO_3^- transport activity was increased in *Xenopus* oocytes expressing NRT1.2^{S292D} (Fig. 6a), but phosphorylated NRT1.2 was unstable both *in vivo and in vitro* assays (Fig. 3, 4). Altogether, our results indicated that NRT1.2 is primarily an ABA rather than a NO_3^- transporter in plants. Alternatively, key phosphorylation sites might differ between the ABA and NO_3^- transport processes. This possibility requires further investigation. However, CEPR2 has been implicated in systemic N-demand signaling (Tabata

et al., 2014). It is possible that, in addition to NRT1.2, CEPR2 might regulate the activities or gene expression of other nitrate transporters. This also needs further investigations.

CEPR2 downregulated ABA signaling and transport by phosphorylating the ABA receptors and transporter

Protein phosphorylation is a rapid and efficient mechanism that regulates the transition between the stress response and growth (Wong et al., 2019; Yang et al., 2019). For example, target of rapamycin (TOR) phosphorylates PYLs to inhibit PYL-ABA binding, suppressing the ABA response. Conversely, increased ABA concentrations under stress conditions stimulate ABA responses to inhibit plant growth (Wang et al., 2018). Similarly, early flowering 1-like (AEL) phosphorylates PYLs to promote PYL ubiquitination and degradation, resulting in the blockage of ABA signaling and the resumption of plant growth (Chen et al., 2018). Recently, we showed that CEPR2 also phosphorylates PYLs to promote PYLs degradation, similarly leading to the suppression of the ABA response under non-stress conditions (Yu et al., 2019). Here, we found that CEPR2 phosphorylated the ABA transporter NRT1.2 and promoted NRT1.2 degradation under normal conditions (Fig. 3, 4). ABA strongly inhibited CEPR2-mediated NRT1.2 phosphorylation and degradation (Fig. 3, 4); non-phosphorylated NRT1.2 imported ABA into cells, which in turn stimulated ABA signaling. Thus, CEPR2-mediated phosphorylation regulates ABA signaling and ABA import to control the transition between the ABA stress response and plant growth under normal condition.

In plants, ABA signaling is crucial for normal growth and the stress response (Kanno et al., 2010; Yang et al., 2019). CEPR2 may act as a key regulator of ABA signaling. Under favorable conditions or upon the cessation of environmental stress, CEPR2 interacts with and phosphorylates PYLs, which accelerates PYLs degradation (Yu et al., 2019). CEPR2-mediated phosphorylation also completely inhibited ABA import activity of NRT1.2,

and hence reduced the importation of ABA into cells under normal condition (Fig. 5a-c). However, the CEPR2-mediated phosphorylation of NRT1.2 caused the degradation of most of the phosphorylated NRT1.2 (Fig. 3, 4). We have reported that the CEPR2-mediated phosphorylation of PYLs was strongly suppressed in the presence of excess ABA (Yu et al., 2019). Also here the CEPR2-mediated phosphorylation of NRT1.2 was strongly suppressed in the presence of excess ABA (Fig. 3, 4). Non-phosphorylated NRT1.2 imported ABA into cells (Fig. 5a-c). These increased concentrations of ABA were recognized by the non-phosphorylated PYLs, eventually stimulating ABA signaling. Thus, CEPR2-mediated phosphorylation finely regulated the ABA response by balancing ABA concentration and ABA signaling. Therefore, CEPR2-mediated phosphorylation represents an important mechanism that maintains the transition between the ABA response and plant growth (Fig. 7). For plant breeding, overexpression of non-phosphorylated NRT1.2 is better than natural type because that it promotes plant growth under both high and low nitrate conditions.

Materials and Methods

Plant materials and growth conditions

Arabidopsis thaliana (L.) Heynh. cv. 'Columbia' was used as the WT. The T-DNA insertion lines, SALK_072696 (*nrt1.2-1*), SALK_011182 (*nrt1.2-2*), and SALK_081193C (*cepr2-2*) in the Col-0 background were obtained from the Arabidopsis Biological Resource Center (http://www.arabidopsis.org). The *cepr2-1* T-DNA insertion mutant and the CEPR2-overexpressing line CEPR2-OE-9 have previously been characterized (Yu et al., 2019). The homozygous single and double mutants, *cepr2-1*, *nrt1.2-1*, and *cepr2-1nrt1.2-1* were verified using RT-PCR with the primers listed in Supplementary Table 2. The *NRT1.2* overexpression seedlings and *nrt1.2-1* complementary seedlings with native promoter-driven *NRT1.2* and point mutant *NRT1.2* at Ser^{292} to alanine which referred as NRT1.2-COMs and $NRT1.2^{S292A}$-COMs were selected on 1/2 Murashige and Skoog (MS) medium (1.5% sucrose

and 0.85% agar) supplemented with 50 mg/L kanamycin. The expression levels of *NRT1.2* and point mutant *NRT1.2* transgenic plants were confirmed using RT-PCR with primers listed in Supplementary Table 2. All selected *Arabidopsis* plants were grown in a greenhouse under a 16 h light/8 h dark cycle at 23°C. The light was 9600 LUX.

Phosphoproteome analysis

Phosphoproteome analysis was performed by capitalBio technology (Beijing, China). For total protein extraction, the TCA/Acetone extraction method was used to isolate total proteins from CEPR2-OE-9 and WT seedlings grown in 1/2 MS for seven days as described by Pi et al (Pi et al., 2016). See Supplementary Figure 1a for a detailed description.

MbSUS, BiFC, and LCI assays

The MbSUS assay was performed as described in a previous study (Obrdlik et al., 2004); detailed descriptions of associated experimental principles and methods were given in a previous study (Yu et al., 2019). In brief, for NubG fusions, PCR products were cloned and transformed with pNXgate, cleaved by *Eco*RI and *Sma*I, into the THY.AP5 yeast strain. Strains were selected on synthetic dropout (SD) medium lacking tryptophan (W) and uracil (U). For CubPLV fusions, pMetYCgate, cleaved with *Pst*I/*Hind*III, was transformed (together with PCR products) into the THY.AP4 yeast strain. Transformants were further selected on SD medium lacking leucine (L). Clones from each transformant were incubated on SD media lacking leucine, tryptophan, and uracil (SD-Trp/-Leu/-Ura; SD-WLU) at 30°C for three days. To detect protein interactions, colonies were spotted onto control media (SD-WLU), as well as onto selection media lacking leucine, tryptophan, uracil, adenine, and histidine (SD-Trp/-Leu/-Ura/-Ade/-His; SD-WLUAH). Colony growth was monitored for 3-6 days.

Luciferase complementary imaging (LCI) assays were performed as previously described (Chen et al., 2008; Xu et al., 2018). In brief, the full-length CDS of *CEPR2* was

371 cloned into the pCAMBIA1300-nLUC (nLUC) vector to generate the CEPR2-nLUC
372 construct, and the full-length CDS of *NRT1.2* was cloned into the pCAMBIA1300-cLUC
373 (cLUC) vector to generate the NRT1.2-cLUC construct. Next, every 1 mL of *A. tumefaciens*
374 cells harboring CEPR2-nLUC, NRT1.2-cLUC, and nLUC were mixed to obtain combinations
375 of CEPR2-nLUC + cLUC, NRT1.2-cLUC + nLUC and CEPR2-nLUC + NRT1.2-cLUC with
376 the final OD_{600} of 1.0. Then the three combinations of combinations of *A. tumefaciens* cells
377 were infiltrated into *N. benthamiana* leaves. Plants were grown at 26°C for 60 h. Five minutes
378 before detection, 0.2 mM luciferin (Promega, Madison, WI, USA) was sprayed on the treated
379 leaves, and luciferase activity was measured using a cooled charge-coupled device (Lumina II,
380 Waltham, MA, USA).

381 BiFC assays were performed as described previously (Waadt and Kudla, 2008). In brief,
382 the full-length CDS without stop codon of *CEPR2* was cloned into the pSPYNE-35S vector to
383 generate the CEPR2-YFP^N construct, while the full-length CDS without stop codon of
384 *NRT1.2* was cloned into the pSPYCE-35S vector to obtain the NRT1.2-YFP^C construct.
385 *Agrobacterium tumefaciens cells* harboring combination of CEPR2-YFP^N and NRT1.2-YFP^C
386 were mixed with 10 mL MMA medium (10 mM $MgCl_2$, 50 mM MES, and 20 μM
387 acetosyringone, pH 5.6) to yield a final optical density at 600 nm (OD_{600}) of 1.0, and was
388 injected into *Nicotiana benthamiana* leaves by gently pressing a disposable syringe to the
389 abaxial surface of a fully-expanded leaf (approximate width of 3 cm at the midpoint). Plants
390 were grown at 26°C for 36–60 h, and then YFP signals of the leaves were detected at 488 nm
391 using a Confocal Laser Scanning Microscope LSM51 (Zeiss, Germany). Here, the
392 amphiphilic styryl dye FM4-64 (N-(3-triethylammomiumpropyl)
393 4-(p-diethylaminophenylhexa-trienyl)) was used as the plasma membrane marker.

394 **Pull down assay**

To characterize the interaction between CEPR2 and NRT1.2, the CDS sequences encoding the cytosol loop region (232–346 aa) of NRT1.2 and the kinase domain (642-977 aa) of CEPR2 were respectively fused with GST and His tag in pGEX-4T-1 and pET30a-His vector to obtain pGEX-4T-1-GST-NRT1.2 (NRT1.2-GST) and pET30a-His-CEPR2^{KD}-His (CEPR2^{KD}-His) constructs. The obtained NRT1.2-GST and CEPR2^{KD}-His constructs were transformed into the competent cells of *E. coli* Rosetta strain. The transformed cells were cultured in 500 mL Luria-Bertani medium at 37°C to an OD_{600} of 1.0. Protein expression was then induced with 0.8 mM Isopropyl β-D-Thiogalactoside (IPTG) for 12 h at 16°C. Next, the *E. coli* cells were obtained by centrifugation at 6000 rpm for 5 min at 4°C and were resuspended in 5 ml ddH_2O. The lysates were obtained using ultrasonication (JY92-II, Scientz Biotechnology Co., Ltd, Ningbo, China) with the following parameters: operating power, 300 w; working time, 10 s; interval time, 5 s; and cycles, 30. Lysates were clarified by centrifugation at 8,000 rpm for 10 min at 4°C. Then, the CEPR2^{KD}-His protein was purified using the His-Tagged Protein Purification Kit (CWBIO, Beijing, China), and NRT1.2-GST was purified using Pierce Glutathione Spin Columns (Thermo, Waltham, MA, USA). In the pull-down assay, 50 μg NRT1.2^{loop}-GST and 50 μg CEPR2^{KD}-His were incubated in 1 mL binding buffer (50 mM Tris-HCl, 150 mM NaCl, pH 8.0) at 4°C for 2 h with constant slight shaking. After incubation, GST proteins were purified with Pierce Glutathione Spin Columns, eluted, and analyzed with anti-His antibodies (CWBIO, Beijing, China). Primers used in this experiment are listed in Supplementary Table 2.

RNA extraction, RT-PCR, and quantitative RT-PCR

Total RNAs from seven-day-old seedlings grown on 1/2 MS with or without 1 μM ABA were extracted using TRIzol (Invitrogen, Carlsbad, CA, USA) or Universal Plant Total RNA Extraction Kits (Spin-column)-I (BioTeke, Beijing, China). The cDNA used for quantitative reverse transcriptase polymerase chain reaction (qRT-PCR) was synthesized using

PrimeScript reverse transcriptase with oligo dT primer using the Prime Script RT Enzyme MIX I (Takara, Osaka, Japan). qRT-PCR analysis was performed with the ChamQ SYBR Color qPCR Master Mix (Q411, Vazyme, Nanjing, China) using a Bio-Rad CFX96 (Bio-Rad, Hercules, CA, USA). *UBC21* and *UBQ10* were used as internal controls for qRT-PCR. The cDNA used for RT-PCR was synthesized using PrimeScript First-Strand cDNA Synthesis Kits (Takara, Osaka, Japan). RT-PCR cycling conditions were as follows: 94°C for 5 min, followed by 23-34 cycles of amplification, and 72°C for 5 min. *EF-1α* was used as the internal control for RT-PCR. The primers used are listed in Supplementary Table 2.

Germination and root length measurements

Plants with different genotypes were grown under same conditions in the greenhouse, and all seeds were harvested simultaneously. Germination assays were performed as previously described (Chen et al., 2014). In brief, the seeds were surface-sterilized and incubated on 1/2 MS medium with or without 1 μM ABA in the dark at 4°C for three days. The germination was calculated every 12 h; germination was defined as the emergence of the radicle through the seed coat. At the end of the three days, germination rates were calculated. To assess growth, sterilized seeds were grown vertically on 1/2 MS medium with or without 1 μM ABA for seven days. The root lengths of at least 20 seedlings of WT, mutant, or transgenic lines were measured using a ruler, and mean root length was calculated.

Cell-free assays

To investigate the effects of CEPR2 on NRT1.2, the protein levels of NRT1.2-GST were detected after incubated with total protein extracts from CEPR2-OE-9, *cepr2-1*, and WT seedling grown on 1/2 MS medium with or without 1 μM ABA. The total proteins of each genotypic plant were extracted from 0.4 g seven-day-old seedlings using 600 μL of extraction buffer (5 mM DTT, 10 mM NaCl, 25 mM Tris-HCl [pH 7.5], 10 mM ATP, 4 mM PMSF, and 10 mM $MgCl_2$). The crude extracts were held on ice (4ºC) for 30 min and centrifuged twice at

12,000 rpm for 10 min at 4°C. After centrifugation, the supernatants were collected. About 0.5 mg of the purified NRT1.2-GST was incubated with the total protein extracts at 22°C for 0, 10, 30, or 60 min. At each time point, 20 μL of each solution was transferred to a new centrifuge tube, combined with 5 μL of 5× loading buffer, and boiled for 5 min to terminate the reaction. The abundance of the NRT1.2 protein in each reaction was detected using anti-GST antibodies. Spot densitometry was measured using ImageJ v1.36 (http://rsb.info.nih.gov/ij/). To investigate the degradation pathway of NRT1.2, protein extracts with 100 μM MG132 (an inhibitor of the 26S proteasome pathway) and/or 100 μM E64d (an inhibitor of the vacuolar degradation pathway) were incubated with purified NRT1.2^{loop}-GST fusion proteins. Protein levels were detected using anti-GST antibodies. ImageJ v1.36 was used to quantify the intensity of each protein band.

In vitro kinase assays

To investigate the possible phosphorylation site NRT1.2 by CEPR2, *in vitro* kinase assays were carried out. The CDS sequences encoding the mutant loop region (232–346 aa) of NRT1.2 at Ser^{277} and Ser^{292} to Alanine (A) or aspartate (D) were respectively fused with GST tag in pGEX-4T-1 vector to obtain pGEX-4T-1-GST-NRT1.2$^{loopS277A/D}$ (NRT1.2$^{loopS277A/D}$-GST) or pGEX-4T-1-GST-NRT1.2$^{loopS292A/D}$ (NRT1.2$^{loopS292A/D}$-GST) constructs. The transformation, induction and purification of fusion proteins were performed as described above. *In vitro* kinase assays were carried out using purified CEPR2^{KD}-His and NRT1.2^{loop}-GST, NRT1.2^{loopS277A}-GST, or NRT1.2^{loopS292A}-GST. We combined 50 μg of NRT1.2^{loop}-GST, NRT1.2^{loopS277A}-GST, or NRT1.2^{loopS292A}-GST with 0.5 μg CEPR2^{KD}-His in 50 μL of reaction buffer (25 mM HEPES, pH 7.2, 1 mM DTT, 50 mM NaCl, 2 mM EGTA, 5 mM $MgSO_4$, and 50 μM ATP). Each reaction mixture was incubated at 30°C for 0 (negative control), 10, 30, or 60 min. Reactions were terminated by adding 12.5 μL 5× loading buffer. NRT1.2 protein levels were quantified with western blot using anti-GST antibodies.

Phosphorylation bands were detected with Mitotic protein monoclonal #2 (MPM-2) antibodies (Albert et al., 2004; Michel et al., 2001). To obtain the effects of ABA on the phosphorylation of NRT1.2, *In vitro* kinase assays were carried out using purified CEPR2^{KD}-His and NRT1.2-GST with or without 10 μM ABA in the presence of 100 μM MG132 and 100 μM E64d. Primers used in this experiment are listed in Supplementary Table 2.

Assays of ABA-import activity in the yeast system

The coding sequences of PYR1 and ABI1 were amplified by PCR and inserted into the pGBKT7 and pGADT7 plasmids, respectively. Then, the plasmids were co-transformed into *Saccharomyces cerevisiae* Yeast Gold cells. Successfully transformed colonies were identified on SD media lacking Leu and Trp (SD-WL). To detect ABA import activity levels, pYES2 plasmids or plasmids containing full length of NRT1.2, NRT1.2^{S292A}, or NRT1.2^{S292D} were transformed into yeast cells, respectively. Successfully transformed colonies were identified on SD-WLU media, then transferred to SD-WLUAH in the absence or presence of 1 μM ABA. ABA-import activity was quantified by observation of growth of transformed cells, because the growth of the transformed yeast cells depend on ABA levels in the cells. Growth photos were taken after culturing for 2-3 days. Yeast transformants were then transferred to 5 mL of SD-WLUAH liquid medium and incubated at 30°C for 8 h in a shaker. The absorbance at 600 nm was measured using a spectrophotometer (T6, Pgeneral, Beijing, China). Twelve replicates for each cotransformant events were carried out. The mean values were obtained. Primers used in this experiment are listed in Supplementary Table 2.

Quantification of NRT1.2 transporter activity in *Xenopus* oocytes

To further test the effects of CEPR2 phosphorylation on NRT1.2-mediated ABA import, we measured the levels of ABA transport activity associated with NRT1.2, nonphosphomimic-NRT1.2 (NRT1.2^{S292A}), and phosphomimic-NRT1.2 (NRT1.2^{S292D}) in the

Xenopus oocytes. The QuikChange Lightning site-directed mutagenesis kit (Agilent Technologies, CA, USA) was used to generate NRT1.2^{S292A} and NRT1.2^{S292D}, which were then cloned into the expression vector pT7TS. The pT7TS plasmids were linearized by *Bam*HI, and the circular RNA (cRNA) was transcribed *in-vitro* using an RNA synthesis kit (mMESSAGE mMACHINET7 kit; Ambion). Primers used in these experiments are listed in Supplementary Table 2. *Xenopus* oocytes were isolated in 25 mL of ND96 solution, containing 43 mg collagenase and 12.5 mg trypsin inhibitor, for 1.5 h. After isolation, cells were recovered in 25 mL of ND96 for another 24 h. *Xenopus* oocytes were then injected with 20 ng of NRT1.2, NRT1.2^{S292A}, NRT1.2^{S292D}, and/or CEPR2^{KD} cRNA. Injected oocytes were incubated in 25 mL NO_3^--free Modified Barth Solution (MBS) (0.71 mM $CaCl_2$, 0.82 mM $MgSO_4$, 1 mM KCl, 2.4 mM $NaHCO_3$, and 15 mM HEPES, 88 mM NaCl, pH 7.4) for 30 h. *Xenopus* oocyte cells injected with the 25 nL water were used as controls. To measure ABA content, *Xenopus* oocytes cells were incubated in MBS with or without 10 μM ABA for 6 h after washed five times with MBS. ABA contents were measured using liquid chromatography-tandem mass spectrometry (LC-MS/MS).

NO_3^- transport activity was also quantified by measuring the NO_3^- incorporated into oocytes using isotope labeling. To measure NO_3^- concentrations in the *Xenopus* oocytes, cells were incubated in 25 mL MBS with $Na^{15}NO_3^-$ for 3 h after washed five times with 25 mL MBS. $^{15}NO_3^-$ levels were measured with an isotope ratio mass spectrometer (IRMS; DELTAplus XP, Thermo, Waltham, MA, USA).

Quantification of NRT1.2 transporter activity *in planta*

To investigate the effects of NRT1.2 phosphorylation on ABA import *in planta*, we first generated transgenic *nrt1.2-1* mutants carrying native promoter-driven normal NRT1.2 (NRT1.2-COMs) or non-phosphorylated NRT1.2 at Ser^{292} (NRT1.2^{S292A}-COMs) described above. For measurement of ABA content, various seedlings including NRT1.2^{S292A}-COM-8,

nrt1.2-1 mutants, NRT1.2-OE-1, and WT grown on 1/2 MS with or without 1 μM ABA for seven days. Next, ABA content in various plants was measured as previous described (Xu et al., 2016). For measurement of NO^{3-} content, different seedlings including NRT1.2^{S292A}-COM-8, NRT1.2-COM-2, *nrt1.2-1*, NRT1.2-OE-1, and WT grown on 2.5 mM succinic diamide liquid medium (10 mM Kpi, pH 5.7, 2.5 mM $(NH_4)_2$Suc, 1 mM $CaCl_2$, 2 mM $MgSO_4$, 1× MN, 0.1 mM $FeNa_2EDTA$, and 1.5% sucrose) for seven days. Next, the seedlings were transferred to 10 mM NO_3^- liquid medium for 0, 0.5, 1, 3, or 5 h. At each time period, 0.05–0.1 g of material (fresh weight) from each seeding was milled into powder using a MM400 (Retsch, Haan, Germany). The powder was mixed with l mL ddH_2O and boiled at 100°C for 30 min. Cooled samples were centrifuged at 13,000 rpm for 10 min, and 400 μL of each supernatant was transferred to a flow cell. NO_3^- content in each cell was detected with the hydrazine reduction method using the AutoAnalyzer 3 continuous flow analytical system, as previously described (Cao et al., 2017).

Author contributions

C.W. and C.Z. conceived the original screening and research plans; Z.Y., L.Z., X.Y., and Y.M. performed experiments, analyzed the data, made the figures, and wrote the original article; G.Y., S.Z., J.H., and K.Y. provided suggestions; C.W. and C.Z. supervised and complemented the writing. All authors read and approved the final manuscript.

Acknowledgments

This work was supported by the National Key R&D Program of China (2018YFD1000704, 2018YFD1000700), the Major Program of Shandong Province Natural Science Foundation (ZR2018ZB0212), and the Natural Science Foundation of China (Grant number 31970292, 31570271). We thank Prof. Yi Wang (Chinese Agricultural University) for the measurement of NRT1.2 transporter activity in *Xenopus* oocyte cells. We also thank LetPub

(https://www.letpub.com/) for its linguistic assistance during the preparation of this manuscript.

Conflict of interest

The authors declare that they have no conflict of interest.

Data availability

All relevant data, vectors, and plant materials that support the findings of this study are available from the corresponding author upon request.

References

Albert, A.L., Lavoie, S.B., and Vincent, M. (2004). Multisite phosphorylation of Pin1-associated mitotic phosphoproteins revealed by monoclonal antibodies MPM-2 and CC-3. BMC Cell Biol 5:22.

Boursiac, Y., Leran, S., Corratge-Faillie, C., Gojon, A., Krouk, G., and Lacombe, B. (2013). ABA transport and transporters. Trends Plant Sci 18:325-333.

Cao, H., Qi, S., Sun, M., Li, Z., Yang, Y., Crawford, N.M., and Wang, Y. (2017). Overexpression of the Maize ZmNLP6 and ZmNLP8 Can Complement the Arabidopsis Nitrate Regulatory Mutant nlp7 by Restoring Nitrate Signaling and Assimilation. Front Plant Sci 8:1703.

Chen, C., Wu, C., Miao, J., Lei, Y., Zhao, D., Sun, D., Yang, G., Huang, J., and Zheng, C. (2014). Arabidopsis SAG protein containing the MDN1 domain participates in seed germination and seedling development by negatively regulating ABI3 and ABI5. J Exp Bot 65:35-45.

Chen, H., Zou, Y., Shang, Y., Lin, H., Wang, Y., Cai, R., Tang, X., and Zhou, J.M. (2008). Firefly luciferase complementation imaging assay for protein-protein interactions in plants. Plant Physiol 146:368-376.

Chen, H.H., Qu, L., Xu, Z.H., Zhu, J.K., and Xue, H.W. (2018). EL1-like Casein Kinases Suppress ABA Signaling and Responses by Phosphorylating and Destabilizing the ABA Receptors PYR/PYLs in Arabidopsis. Mol Plant 11:706-719.

Cutler, S.R., Rodriguez, P.L., Finkelstein, R.R., and Abrams, S.R. (2010). Abscisic acid: emergence of a core signaling network. Annu Rev Plant Biol 61:651-679.

Huang, N.C., Liu, K.H., Lo, H.J., and Tsay, Y.F. (1999). Cloning and functional characterization of an Arabidopsis nitrate transporter gene that encodes a constitutive component of low-affinity uptake. Plant Cell 11:1381-1392.

Kang, J., Yim, S., Choi, H., Kim, A., Lee, K.P., Lopez-Molina, L., Martinoia, E., and Lee, Y. (2015). Abscisic acid transporters cooperate to control seed germination. Nat Commun 6:8113.

Kanno, Y., Hanada, A., Chiba, Y., Ichikawa, T., Nakazawa, M., Matsui, M., Koshiba, T., Kamiya, Y., and Seo, M. (2012). Identification of an abscisic acid transporter by functional screening using the receptor complex as a sensor. Proc Natl Acad Sci U S A 109:9653-9658.

Kanno, Y., Jikumaru, Y., Hanada, A., Nambara, E., Abrams, S.R., Kamiya, Y., and Seo, M. (2010). Comprehensive hormone profiling in developing Arabidopsis seeds: examination of the site of ABA biosynthesis, ABA transport and hormone interactions. Plant Cell Physiol 51:1988-2001.

Kanno, Y., Kamiya, Y., and Seo, M. (2013). Nitrate does not compete with abscisic acid as a substrate of AtNPF4.6/NRT1.2/AIT1 in Arabidopsis. Plant Signal Behav 8:e26624.

Kuromori, T., Miyaji, T., Yabuuchi, H., Shimizu, H., Sugimoto, E., Kamiya, A., Moriyama, Y., and Shinozaki, K. (2010). ABC transporter AtABCG25 is involved in abscisic acid transport and responses. Proc Natl Acad Sci U S A 107:2361-2366.

Li, W., Song, T., Wallrad, L., Kudla, J., Wang, X., and Zhang, W. (2019). Tissue-specific accumulation of pH-sensing phosphatidic acid determines plant stress tolerance. Nat Plants 5:1012-1021.

Michel, L.S., Liberal, V., Chatterjee, A., Kirchwegger, R., Pasche, B., Gerald, W., Dobles, M., Sorger, P.K., Murty, V.V., and Benezra, R. (2001). MAD2 haplo-insufficiency causes premature anaphase and chromosome instability in mammalian cells. Nature 409:355-359.

Obrdlik, P., El-Bakkoury, M., Hamacher, T., Cappellaro, C., Vilarino, C., Fleischer, C., Ellerbrok, H., Kamuzinzi, R., Ledent, V., Blaudez, D., et al. (2004). K+ channel interactions detected by a genetic system optimized for systematic studies of membrane protein interactions. Proc Natl Acad Sci U S A 101:12242-12247.

Pi, E., Qu, L., Hu, J., Huang, Y., Qiu, L., Lu, H., Jiang, B., Liu, C., Peng, T., Zhao, Y., et al. (2016). Mechanisms of Soybean Roots' Tolerances to Salinity Revealed by Proteomic

and Phosphoproteomic Comparisons Between Two Cultivars. Mol Cell Proteomics 15:266-288.
Raghavendra, A.S., Gonugunta, V.K., Christmann, A., and Grill, E. (2010). ABA perception and signalling. Trends Plant Sci 15:395-401.
Soma, F., Mogami, J., Yoshida, T., Abekura, M., Takahashi, F., Kidokoro, S., Mizoi, J., Shinozaki, K., and Yamaguchi-Shinozaki, K. (2017). ABA-unresponsive SnRK2 protein kinases regulate mRNA decay under osmotic stress in plants. Nat Plants 3:16204.
Tabata, R., Sumida, K., Yoshii, T., Ohyama, K., Shinohara, H., and Matsubayashi, Y. (2014). Perception of root-derived peptides by shoot LRR-RKs mediates systemic N-demand signaling. Science 346:343-346.
Teardo, E., Carraretto, L., Moscatiello, R., Cortese, E., Vicario, M., Festa, M., Maso, L., De Bortoli, S., Cali, T., Vothknecht, U.C., et al. (2019). A chloroplast-localized mitochondrial calcium uniporter transduces osmotic stress in Arabidopsis. Nat Plants 5:581-588.
Waadt, R., and Kudla, J. (2008). In Planta Visualization of Protein Interactions Using Bimolecular Fluorescence Complementation (BiFC). CSH Protoc 2008:pdb prot4995.
Wang, P., Zhao, Y., Li, Z., Hsu, C.C., Liu, X., Fu, L., Hou, Y.J., Du, Y., Xie, S., Zhang, C., et al. (2018). Reciprocal Regulation of the TOR Kinase and ABA Receptor Balances Plant Growth and Stress Response. Mol Cell 69:100-112 e106.
Wong, M.M., Bhaskara, G.B., Wen, T.N., Lin, W.D., Nguyen, T.T., Chong, G.L., and Verslues, P.E. (2019). Phosphoproteomics of Arabidopsis Highly ABA-Induced1 identifies AT-Hook-Like10 phosphorylation required for stress growth regulation. Proc Natl Acad Sci U S A 116:2354-2363.
Xu, Q., Truong, T.T., Barrero, J.M., Jacobsen, J.V., Hocart, C.H., and Gubler, F. (2016). A role for jasmonates in the release of dormancy by cold stratification in wheat. J Exp Bot 67:3497-3508.
Xu, Y., Yu, Z., Zhang, D., Huang, J., Wu, C., Yang, G., Yan, K., Zhang, S., and Zheng, C. (2018). CYSTM, a Novel Non-Secreted Cysteine-Rich Peptide Family, Involved in Environmental Stresses in Arabidopsis thaliana. Plant Cell Physiol 59:423-438.
Yang, G., Yu, Z., Gao, L., and Zheng, C. (2019). SnRK2s at the Crossroads of Growth and Stress Responses. Trends Plant Sci 24:672-676.
Yu, Z., Zhang, D., Xu, Y., Jin, S., Zhang, L., Zhang, S., Yang, G., Huang, J., Yan, K., Wu, C., et al. (2019). CEPR2 phosphorylates and accelerates the degradation of PYR/PYLs in Arabidopsis. J Exp Bot.
Zhang, H., Li, Y., and Zhu, J.K. (2018). Developing naturally stress-resistant crops for a sustainable agriculture. Nat Plants 4:989-996.
Zhang, H., Zhu, H., Pan, Y., Yu, Y., Luan, S., and Li, L. (2014). A DTX/MATE-type transporter facilitates abscisic acid efflux and modulates ABA sensitivity and drought tolerance in Arabidopsis. Mol Plant 7:1522-1532.

Supplementary data

Supplementary Figure 1. Phosphoproteome analysis and MbSUS assay to detect the interaction between CEPR2 and the 78 proteins with upregulated phosphorylation

Supplementary Figure 2. The transcription level of different ABA transporters in CEPR2-OE-9, WT, and *cepr2-1* seedlings with or without ABA were examined by qRT-PCR

Supplementary Figure 3. Structure prediction of NRT1.2 protein

Supplementary Figure 4. The optimizing codon sequence of loop domain of NRT1.2

Supplementary Figure 5. The phosphorylation of NRT1.2 did not affect the interaction with CEPR2

Supplementary Figure 6. Selection of the optimal ABA concentration in Y2H system

Supplementary Figure 7. Construction of the complementary materials of *nrt1.2-1*

Supplementary Table 1. The 78 dramatically upregulated phosphoproteins identified in phosphorylation mass spectrometry

Supplementary Table 2. The primers used in this study

Supplementary Excel 1. The peptides differentially phosphorylated between CEPR2-OE-9 and WT seedlings identified by mass spectrometry

Figure legends

Figure 1. CEPR2 interacts with the ABA importer NRT1.2. (a) Firefly luciferase complementation imaging assay, showing interactions between CEPR2 and NRT1.2. A key to the combination shown in each quadrant is given above the image. **(b)** Bimolecular fluorescence complementation assay, showing the interaction between CEPR2 and NRT1.2 in *Nicotiana benthamiana*. FM4-64: plasma membrane dye, N-(3-triethylammomiumpropyl) 4-(p-diethylaminophenylhexa-trienyl). **(c)** The protein structure of CEPR2 and NRT1.2. The phosphorylation sites S277 and S292 identified by phosphorylation mass spectrometry were labeled in NRT1.2 protein. LRR, leucine-rich repeat receptor-like domain; KD, kinase domain; Loop, loop domain of NRT1.2; PM, plasma membrane. **(d)** MbSUS assay showing the functional domains of CEPR2 that interact with the loop region of NRT1.2 ($NRT1.2^{loop}$, 232-346 aa). **(e)** Pull down assays using purified GST, $NRT1.2^{loop}$-GST, and $CEPR2^{KD}$-His expressed in *E.coli*. **(f)** Mating-based split ubiquitin system assay (MbSUS) to detect the interaction between CEPR2 and various ABA importers, including NRT1.2, ABA importer 2

675 (AIT2), AIT3, AIT4, ABC transporter G25 (ABCG25), ABCG30, ABCG31, and ABCG40.

676 **Figure 2. CEPR2 acts NRT1.2 epistatically to affect ABA signaling. (a)** *NRT1.2* transcript
677 levels and protein levels in WT and transgenic *Arabidopsis* lines overexpressing NRT1.2
678 detected by RT-PCR and western blot. *EF-1α* was used as the internal control for RT-PCR,
679 and Rubisco large protein (RbcL) was used as a loading control for the western blot. **(b)**
680 Schematic illustration of T-DNA insertion sites for the *nrt1.2-1* and *nrt1.2-2* mutants. **(c)**
681 *NRT1.2* transcript levels and protein levels in WT, *nrt1.2-1*, and *nrt1.2-2* seedlings. **(d)**
682 Phenotypes of the WT, NRT1.2-OE, *nrt1.2-1*, *nrt1.2-2*, *cepr2-1*, and *cepr2-1nrt1.2-1*
683 seedlings grown for seven days on 1/2 MS with or without 1 μM ABA. **(e)** Lengths of the
684 primary roots of the seedlings shown in (d). Error bars indicate SEM (N = 3). Bars labeled
685 with different lowercase letters are significantly different from one another ($P < 0.05$; one
686 way ANOVA). **(f)** The germination rates of the seedlings shown in (d). Error bars indicate
687 SEM (N = 3).

688 **Figure 3. CEPR2 reduces NRT1.2 stability via the 26S proteasome pathway and the**
689 **vacuolar degradation pathway. (a)** The cell-free degradation of NRT1.2-GST in soluble
690 protein extracts of CEPR2-OE-9, WT, and *cepr2-1* seedlings treated with or without 1 μM
691 ABA. NRT1.2^{loop}-GST protein levels were quantified using anti-GST antibody in western blot
692 as indicated by red arrows. **(b)** Normalized plot of the NRT1.2 degradation shown in (a),
693 based on the band intensity quantified by ImageJ. Error bars indicate SEM (N = 3). **(c)** The
694 cell-free degradation of NRT1.2^{loop}-GST and NRT1.2^{loopS292A}-GST protein in the soluble
695 protein extracts from seven-day-old CEPR2-OE-9 seedlings grown on 1/2 MS medium with
696 or without 100 μM MG132 (an inhibitor of the 26S proteasome degradation pathway), and/or
697 100 μM E64d (an inhibitor of the vacuolar degradation pathway) for 0, 0.5, 1, and 2 h.
698 NRT1.2^{loop}-GST protein levels were quantified using anti-GST antibody in western blots as
699 indicated by red arrows. RbcL was used as the loading control.

Figure 4. CEPR2 reduces NRT1.2 stability depending on the phosphorylation of Serine 292 (Ser^{292}). (a) *In vitro* kinase assays showing the phosphorylation effect of CEPR2 on the loop regions of NRT1.2 (NRT1.2^{loop}-GST), NRT1.2^{loop} with Ser^{277} mutated to alanine (A) (NRT1.2^{loopS277A}-GST), and NRT1.2^{loop} with Ser^{292} mutated to A (NRT1.2^{loopS292A}-GST). NRT1.2 phosphorylation status was detected by the MPM-2 antibody. **(b)** *In vitro* kinase assays showing the effects of 10 μM ABA on the phosphorylation of NRT1.2^{loop}-GST. MG132 and E64d were used to block the degradation of NRT1.2. **(c)** Cell-free degradation assays showing the effects of ABA on the degradation of NRT1.2^{loop} and NRT1.2^{loopS292A} in the soluble protein extract from CEPR2-OE-9 seedlings. NRT1.2^{loop}-GST and NRT1.2^{loopS292A}-GST were quantified using western blot with the anti-GST antibody. RbcL was used as the loading control.

Figure 5. If Ser^{292} is not phosphorylated, NRT1.2 imports ABA. (a) Y2H assays showing the ABA transporter activity of NRT1.2. pYES2-NRT1.2 represent normal NRT1.2. pYES2-NRT1.2^{S277A}, -NRT1.2^{S277D}, -NRT1.2^{S292A}, -NRT1.2^{S292D}, -NRT1.2^{S277AS292A}, and -NRT1.2^{S277DS292D} represent nonphosphorylated and phosphorylated NRT1.2 obtained by point mutant at Ser^{277} and Ser^{292} to alanine (A) and aspartate (D). pYES2 empty vector was used as control. **(b)** Optical densities (OD) at 600 nm of the independent transformants yeast cells. Error bars indicate SEM (N = 3). Bars labeled with different lowercase letters are significantly different from one another (P < 0.05; one way ANOVA). **(c)** ABA-import activity in *Xenopus* oocytes expressing NRT1.2, NRT1.2^{S292A}, NRT1.2^{S292D}, CEPR2^{KD}, or NRT1.2 plus CEPR2^{KD}. *Xenopus* oocytes injected with water were used as negative control. Error bars indicate SEM (N = 3). Statistically significant differences were identified between pairs of measurements using Student's t-test (***P < 0.001; ns, no significance). **(d)** Various genotype seedlings including WT, *nrt1.2-1*, NRT1.2-OE-1, NRT1.2-COM-1, and NRT1.2^{S292A}-COMs seedlings grown on 1/2 MS with or without 1 μM ABA for seven days. Error bars indicate SEM (N = 3). Statistically significant differences were identified between

726 pairs of measurements using Student's *t*-test (**$P < 0.01$). **(e)** ABA contents in WT, *nrt1.2-1*,
727 NRT1.2-OE-1, and NRT1.2^{S292A}-COM-8 seedlings grown on 1/2 MS or 1 μM ABA for seven
728 days. Error bars indicate SEM ($N = 3$). Bars labeled with different lowercase letters are
729 significantly different from one another ($P < 0.05$; one way ANOVA). **(f)** NRT1.2 protein
730 levels in WT, NRT1.2-COMs, and NRT1.2^{S292A}-COMs seedlings grown on 1/2 MS with or
731 without 1 μM ABA for seven days detected using western blots. RbcL was used as the loading
732 control.

733 **Figure 6. Phosphorylation at Ser^{292} slightly increases the NO_3^--import activity of NRT1.2.**
734 **(a)** NO_3^--import activity in *Xenopus* oocytes expressing NRT1.2, CEPR2^{KD}, NRT1.2^{S292A},
735 NRT1.2^{S292D}, or NRT1.2 plus CEPR2^{KD}. *Xenopus* oocytes injected with water were used as
736 negative control. Error bars indicate SEM ($N = 3$). Bars labeled with different lowercase
737 letters are significantly different from one another ($P < 0.05$; one way ANOVA). **(b)** NO_3^-
738 contents in WT, *nrt1.2-1*, NRT1.2-OE-1, NRT1.2-COM-2, and NRT1.2^{S292A}-COM-8
739 seedlings grown on succinic diamide liquid medium for seven days, and then transferred to
740 succinic diamide liquid medium supplemented with 10 mM NO_3^- for NO_3^-transport activity
741 detection. FW, fresh weight. Error bars indicate SEM ($N = 3$). **(c)** Various genotype seedlings
742 grown on high-nitrogen (10 mM NO_3^-) or low-nitrogen (0.25 mM NO_3^-) medium for ten days.
743 **(d and e)** The primary root length **(d)** and the fresh weight **(e)** of various genotype seedlings
744 grown on high-nitrogen (10 mM NO_3^-) or low-nitrogen (0.25 mM NO_3^-) medium for ten days.
745 Error bars indicate SEM ($N = 3$). Bars labeled with different lowercase letters are significantly
746 different from one another ($P < 0.01$; one way ANOVA).

747 **Figure 7. The CEPR2-mediated phosphorylation of NRT1.2 and PYLs balances growth**
748 **and the ABA response in *Arabidopsis*.** Under normal conditions, CEPR2 interacts with and
749 phosphorylates PYLs, leading to degradation and the suppression of ABA signaling.
750 Simultaneously, CEPR2 interacts with and phosphorylates NRT1.2, completely inhibiting

ABA-import and stimulating NRT1.2 degradation. Thus, CEPR2 suppresses the ABA response by regulating ABA signaling and ABA import. Along with the environmental stimuli that result in ABA accumulation, ABA import and the ABA response are increased because ABA inhibits the phosphorylation of PYLs and NRT1.2, stabilizing PYLs and NRT1.2, and thus restoring the ABA binding ability of PYLs, as well as the ABA-importing activity of NRT1.2.

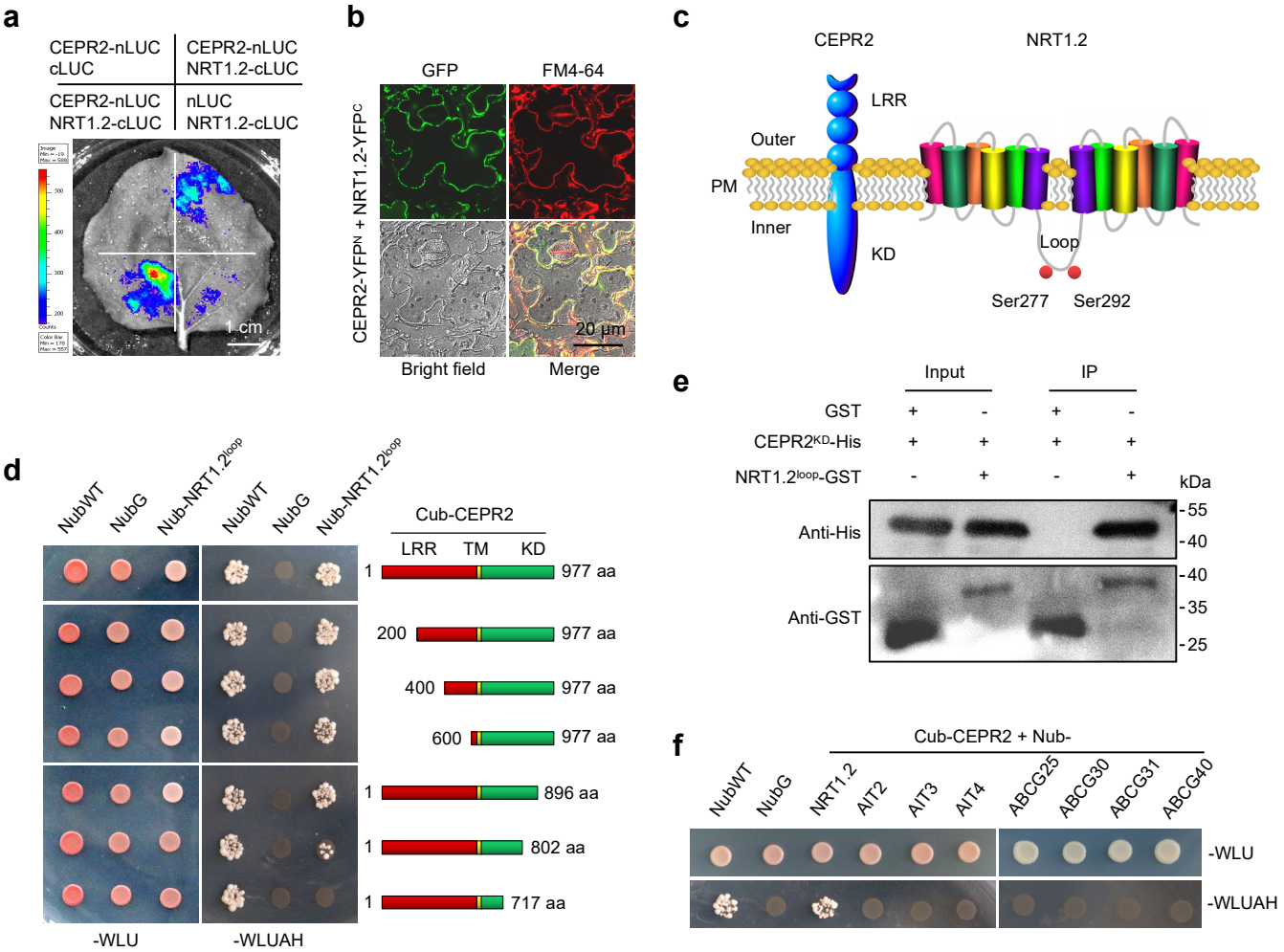

Figure 1. CEPR2 interacts with the ABA importer NRT1.2. (a) Firefly luciferase complementation imaging assay, showing interactions between CEPR2 and NRT1.2. A key to the combination shown in each quadrant is given above the image. **(b)** Bimolecular fluorescence complementation assay, showing the interaction between CEPR2 and NRT1.2 in *Nicotiana benthamiana*. FM4-64: plasma membrane dye, N-(3-triethylammomiumpropyl) 4-(p-diethylaminophenylhexa-trienyl). **(c)** The protein structure of CEPR2 and NRT1.2. The phosphorylation sites S277 and S292 identified by phosphorylation mass spectrometry were labeled in NRT1.2 protein. LRR, leucine-rich repeat receptor-like domain; KD, kinase domain; Loop, loop domain of NRT1.2; PM, plasma membrane. **(d)** MbSUS assay showing the functional domains of CEPR2 that interact with the loop region of NRT1.2 ($NRT1.2^{loop}$, 232–346 aa). **(e)** Pull down assays using purified GST, $NRT1.2^{loop}$-GST, and $CEPR2^{KD}$-His expressed in *E.coli*. **(f)** Mating-based split ubiquitin system assay (MbSUS) to detect the interaction between CEPR2 and various ABA importers, including NRT1.2, ABA importer 2 (AIT2), AIT3, AIT4, ABC transporter G25 (ABCG25), ABCG30, ABCG31, and ABCG40.

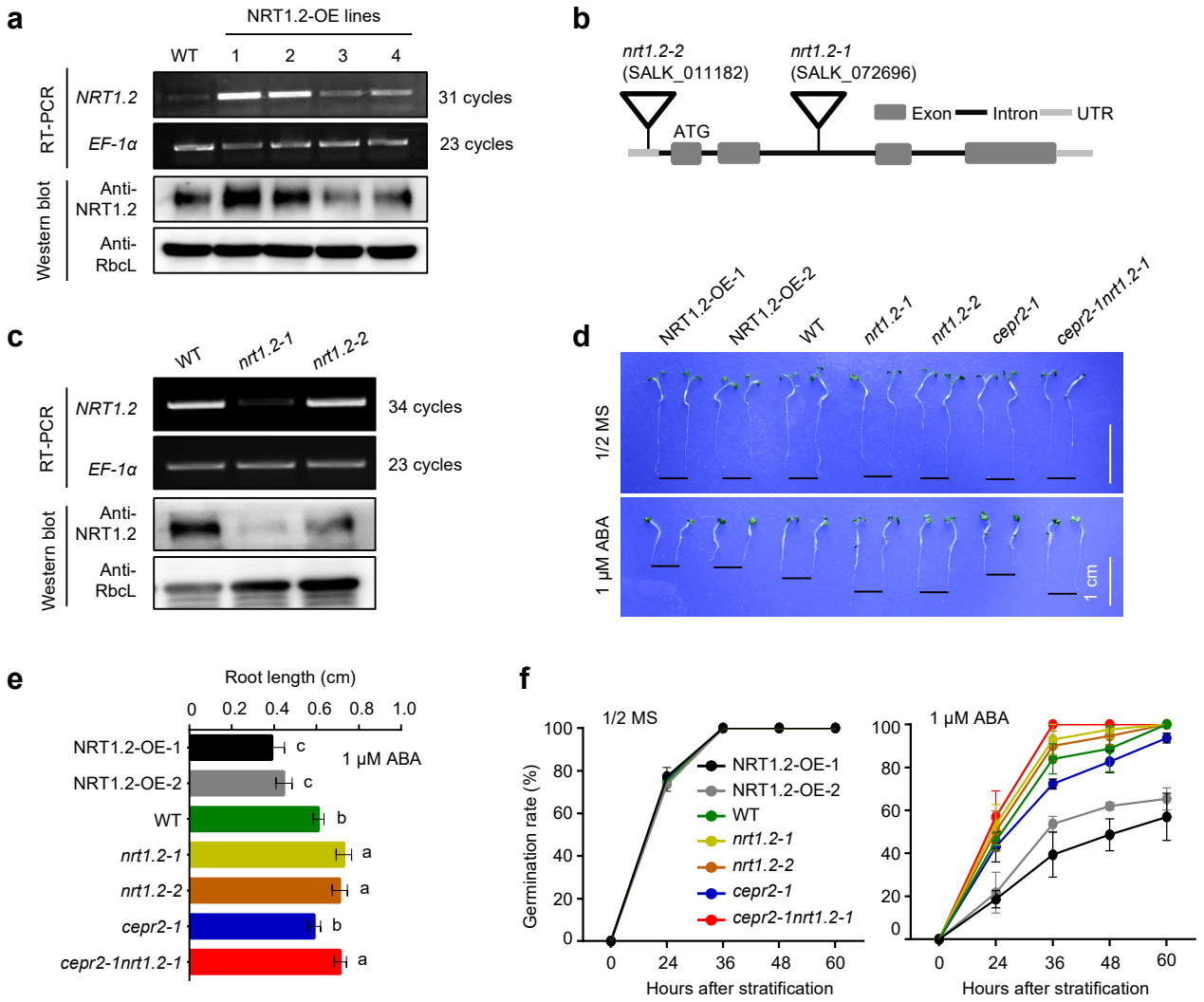

Figure 2. CEPR2 acts NRT1.2 epistatically to affect ABA signaling.

(a) *NRT1.2* transcript levels and protein levels in WT and transgenic *Arabidopsis* lines overexpressing NRT1.2 detected by RT-PCR and western blot. *EF-1α* was used as the internal control for RT-PCR, and Rubisco large protein (RbcL) was used as a loading control for the western blot. **(b)** Schematic illustration of T-DNA insertion sites for the *nrt1.2-1* and *nrt1.2-2* mutants. **(c)** *NRT1.2* transcript levels and protein levels in WT, *nrt1.2-1*, and *nrt1.2-2* seedlings. **(d)** Phenotypes of the WT, NRT1.2-OE, *nrt1.2-1*, *nrt1.2-2*, *cepr2-1*, and *cepr2-1nrt1.2-1* seedlings grown for seven days on 1/2 MS with or without 1 μM ABA. **(e)** Lengths of the primary roots of the seedlings shown in (d). Error bars indicate SEM (N = 3). Bars labeled with different lowercase letters are significantly different from one another (P < 0.05; one way ANOVA). **(f)** The germination rates of the seedlings shown in (d). Error bars indicate SEM (N = 3).

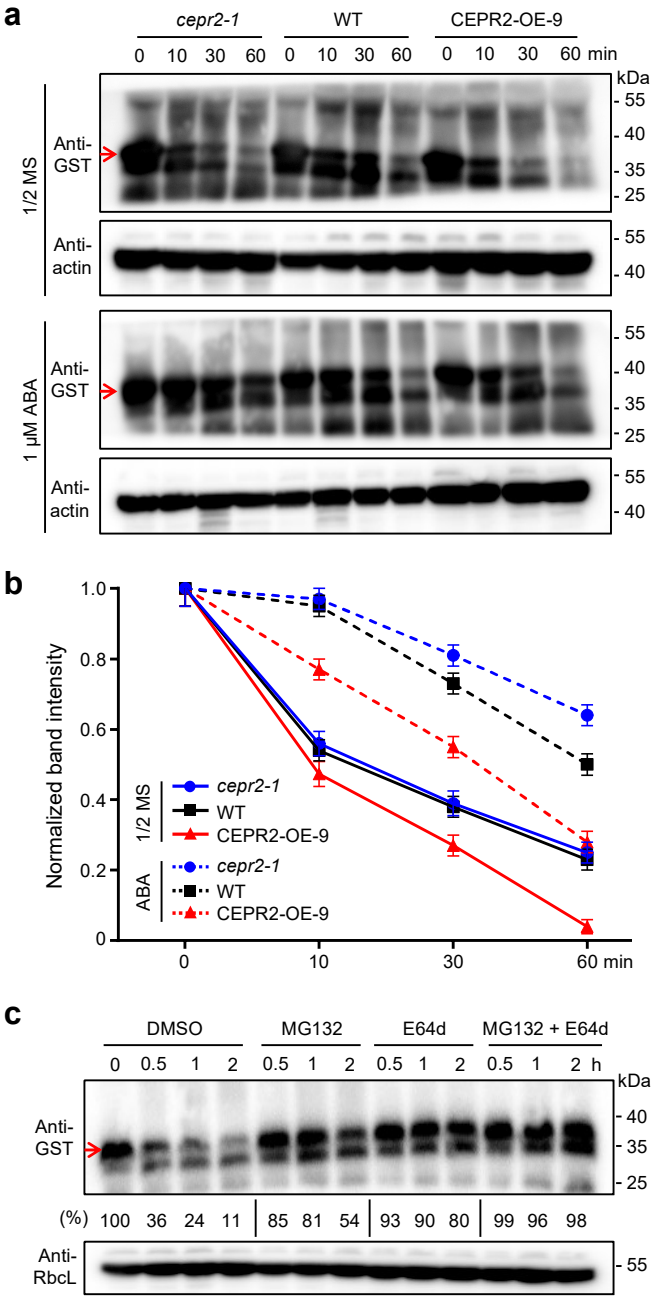

Figure 3. CEPR2 reduces NRT1.2 stability via the 26S proteasome pathway and the vacuolar degradation pathway.

(a) The cell-free degradation of NRT1.2-GST in soluble protein extracts of CEPR2-OE-9, WT, and *cepr2-1* seedlings treated with or without 1 μM ABA. NRT1.2^{loop}-GST protein levels were quantified using anti-GST antibody in western blots as indicated by red arrows. **(b)** Normalized plot of the NRT1.2 degradation shown in (a), based on the band intensity quantified by ImageJ as described in methods. Error bars indicate SEM (N = 3). **(c)** The cell-free degradation of NRT1.2^{loop}-GST and NRT1.2^{loopS292A}-GST protein in the soluble protein extracts from seven-day-old CEPR2-OE-9 seedlings grown on 1/2 MS medium with or without 100 μM MG132 (an inhibitor of the 26S proteasome degradation pathway), and/or 100 μM E64d (an inhibitor of the vacuolar degradation pathway) for 0, 0.5, 1, and 2 h. NRT1.2^{loop}-GST protein levels were quantified using anti-GST antibody in western blots as indicated by red arrows. RbcL was used as the loading control.

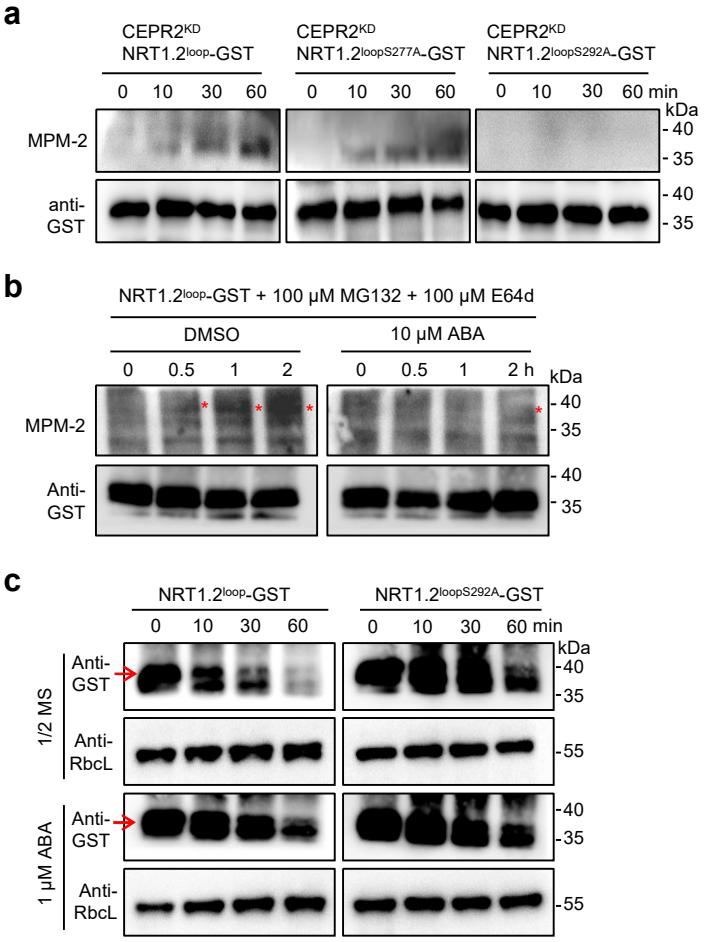

Figure 4. CEPR2 reduces NRT1.2 stability depending on the phosphorylation of Serine 292 (Ser^{292}).

(a) *In vitro* kinase assays showing the phosphorylation effect of CEPR2 on the loop regions of NRT1.2 (NRT1.2^{loop}-GST), NRT1.2^{loop} with Ser^{277} mutated to alanine (A) (NRT1.2^{loopS277A}-GST), and NRT1.2^{loop} with Ser^{292} mutated to A (NRT1.2^{loopS292A}-GST). NRT1.2 phosphorylation status was detected by the MPM-2 antibody. **(b)** *In vitro* kinase assays showing the effects of 10 μM ABA on the phosphorylation of NRT1.2^{loop}-GST. MG132 and E64d were used to block the degradation of NRT1.2. **(c)** Cell-free degradation assays showing the effects of ABA on the degradation of NRT1.2^{loop} and NRT1.2^{loopS292A} in the soluble protein extract from CEPR2-OE-9 seedlings. NRT1.2^{loop}-GST and NRT1.2^{loopS292A}-GST were quantified using western blot with the anti-GST antibody. RbcL was used as the loading control.

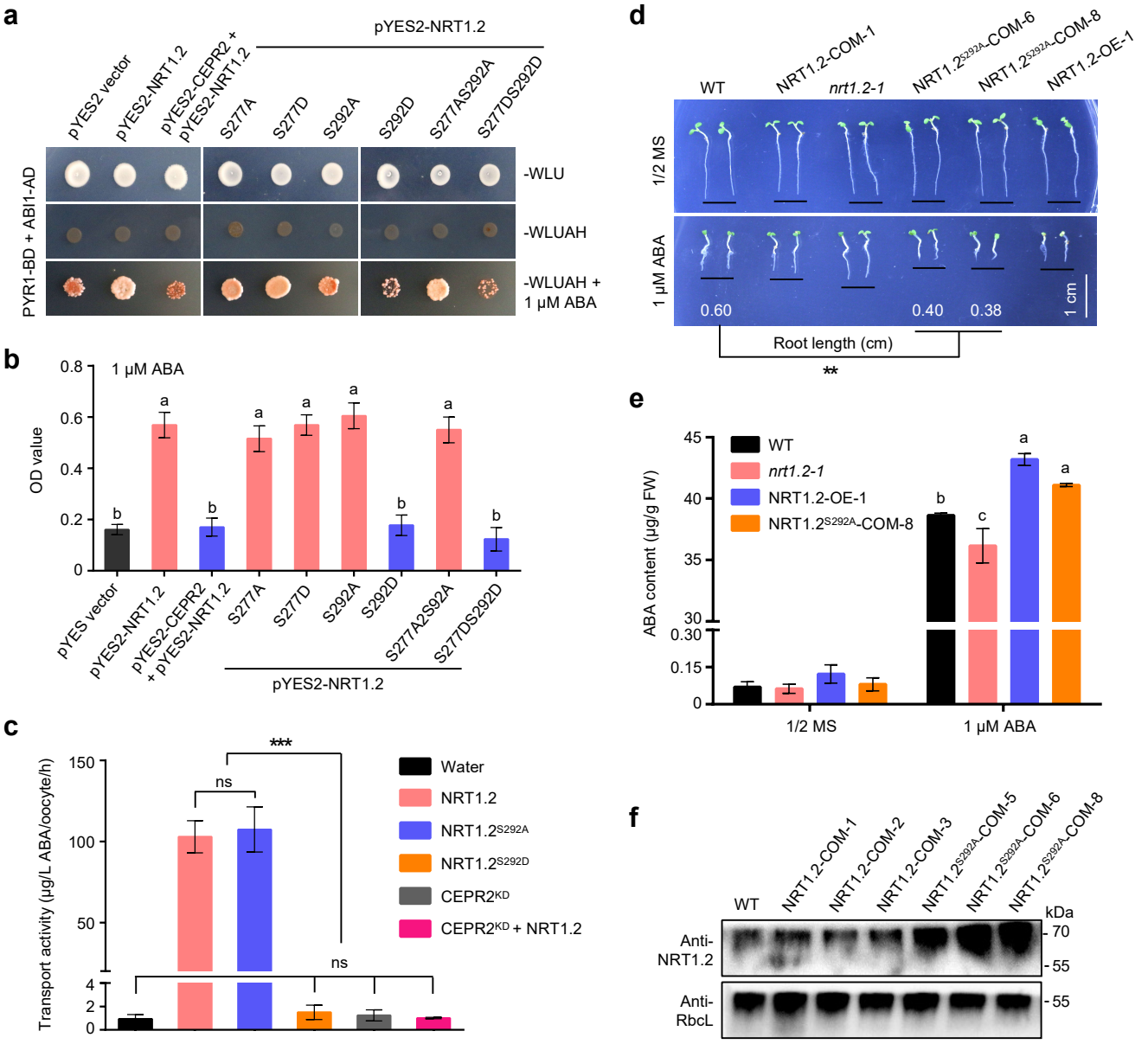

Figure 5. If Ser292 is not phosphorylated, NRT1.2 imports ABA.

(a) Y2H assays showing the ABA transporter activity of NRT1.2. pYES2-NRT1.2 represent normal NRT1.2. pYES2-NRT1.2^{S277A}, -NRT1.2^{S277D}, -NRT1.2^{S292A}, -NRT1.2^{S292D}, -NRT1.2^{S277AS292A}, and -NRT1.2^{S277DS292D} represent nonphosphorylated and phosphorylated NRT1.2 obtained by point mutant at Ser^{277} and Ser^{292} to alanine (A) and aspartate (D). pYES2 empty vector was used as control. **(b)** Optical densities (OD) at 600 nm of the independent transformants yeast cells. Error bars indicate SEM (N = 3). Bars labeled with different lowercase letters are significantly different from one another (P < 0.05; one way ANOVA). **(c)** ABA-import activity in *Xenopus* oocytes expressing NRT1.2, NRT1.2^{S292A}, NRT1.2^{S292D}, CEPR2^{KD}, or NRT1.2 plus CEPR2^{KD}. *Xenopus* oocytes injected with water were used as negative control. Error bars indicate SEM (N = 3). Statistically significant differences were identified between pairs of measurements using Student's *t*-test (***P < 0.001; ns, no significance). **(d)** Various genotype seedlings including WT, *nrt1.2-1*, NRT1.2-OE-1, NRT1.2^{S292A}-COM-8 seedlings grown on 1/2 MS with or without 1 μM ABA for seven days. Error bars indicate SEM (N = 3). Statistically significant differences were identified between pairs of measurements using Student's *t*-test (**P < 0.01). **(e)** ABA contents in WT, *nrt1.2-1*, NRT1.2-OE-1, and NRT1.2^{S292A}-COM-8 seedlings grown on 1/2 MS or 1 μM ABA for seven days. Error bars indicate SEM (N = 3). Bars labeled with different lowercase letters are significantly different from one another (P < 0.05; one way ANOVA). **(f)** NRT1.2 protein levels in WT, NRT1.2-COM-1s, and NRT1.2^{S292A}-COMs seedlings grown on 1/2 MS with or without 1 μM ABA for seven days detected using western blots. RbcL was used as the loading control.

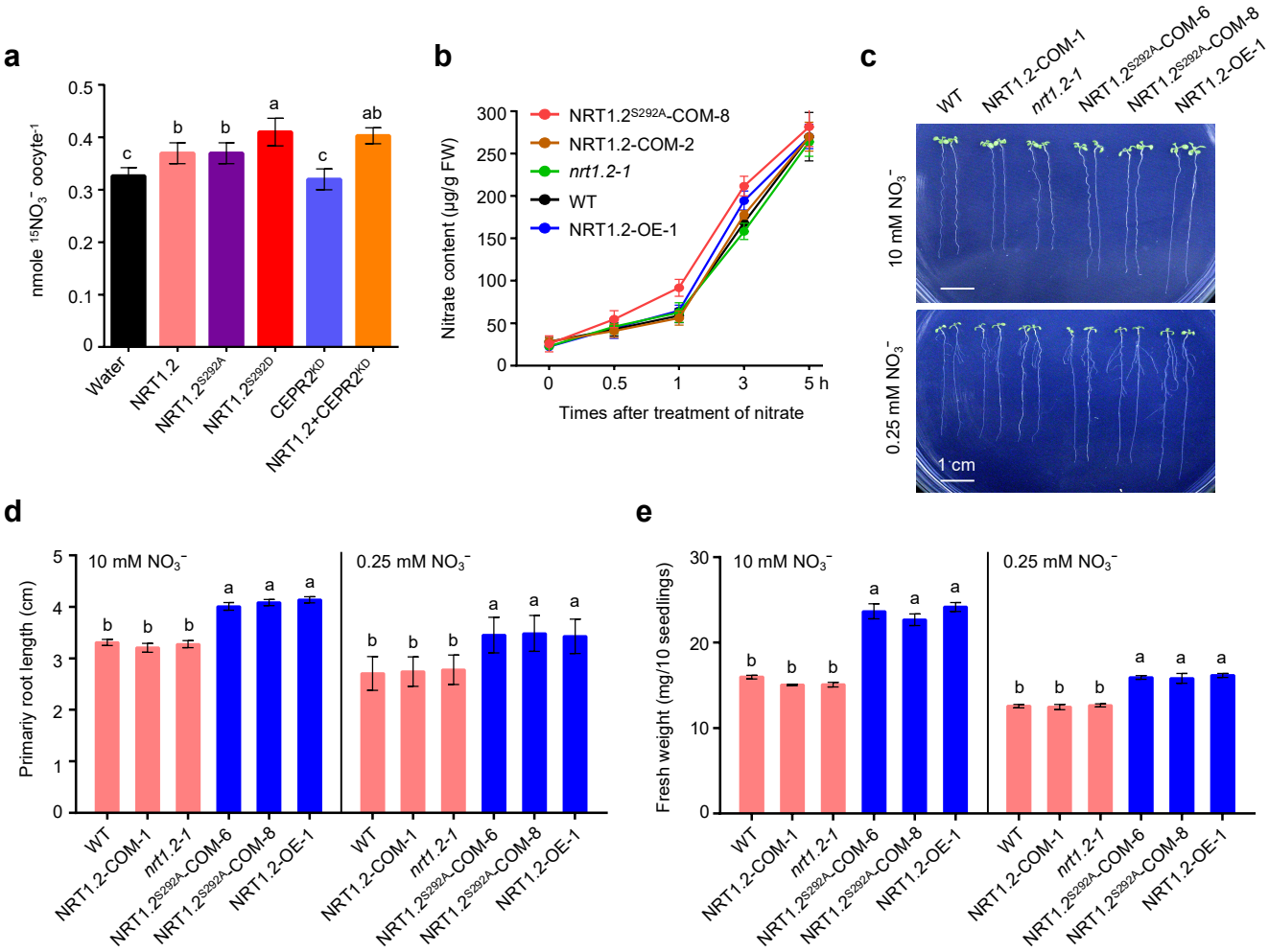

Figure 6. Phosphorylation at Ser^{292} slightly increases the NO_3^--import activity of NRT1.2.

(a) NO_3^--import activity in *Xenopus* oocytes expressing NRT1.2, CEPR2^{KD}, NRT1.2^{S292A}, NRT1.2^{S292D}, or NRT1.2 plus CEPR2^{KD}. *Xenopus* oocytes injected with water were used as negative control. Error bars indicate SEM (N = 3). Bars labeled with different lowercase letters are significantly different from one another (P < 0.05; one way ANOVA). **(b)** NO_3^- contents in WT, *nrt1.2-1*, NRT1.2-OE-1, NRT1.2-COM-2, and NRT1.2^{S292A}-COM-8 seedlings grown on succinic diamide liquid medium for seven days, and then transferred to succinic diamide liquid medium supplemented with 10 mM NO_3^- for NO_3^- transport activity detection. FW, fresh weight. Error bars indicate SEM (N = 3). **(c)** Various genotype seedlings grown on high-nitrogen (10 mM NO_3^-) or low-nitrogen (0.25 mM NO_3^-) medium for ten days. **(d** and **e)** The primary root length **(d)** and the fresh weight **(e)** of various genotype seedlings grown on high-nitrogen (10 mM NO_3^-) or low-nitrogen (0.25 mM NO_3^-) medium for ten days. Error bars indicate SEM (N = 3). Bars labeled with different lowercase letters are significantly different from one another (P < 0.01; one way ANOVA).

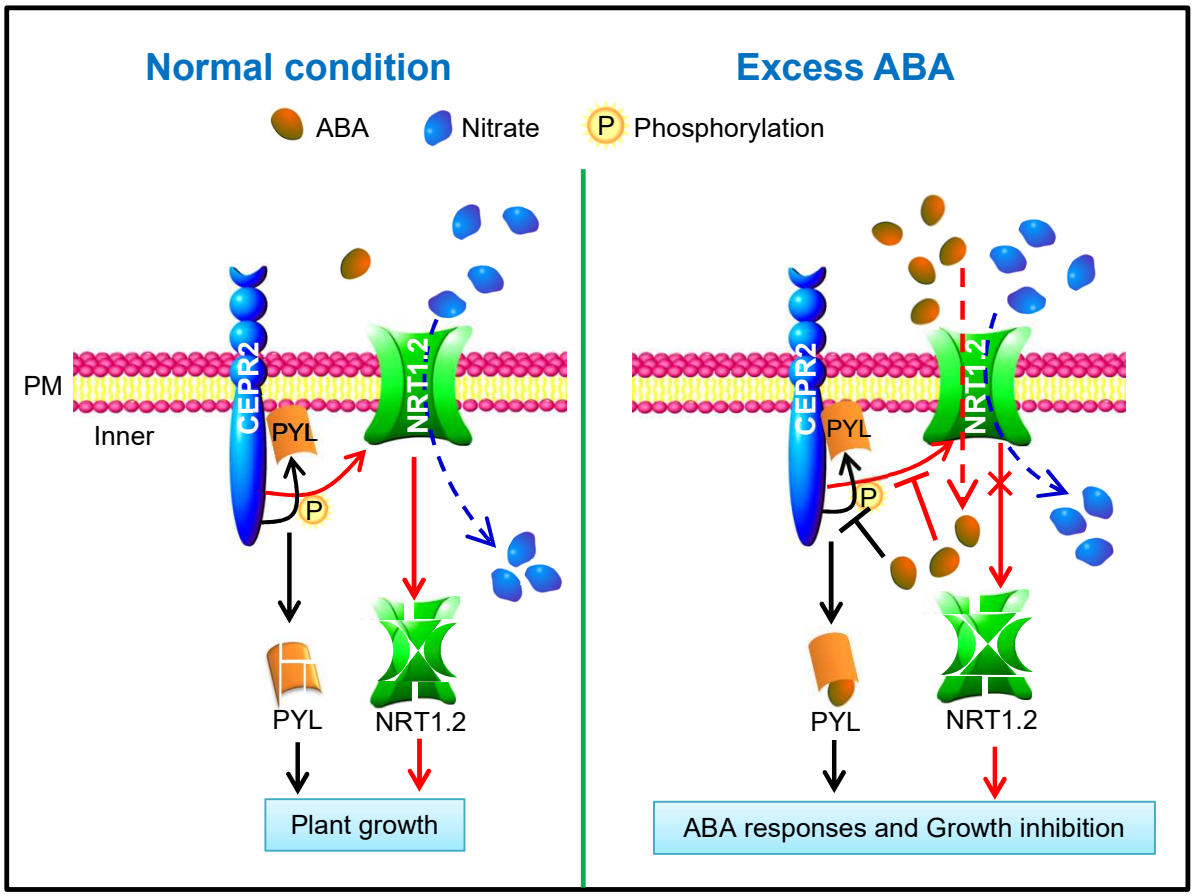

Figure 7. The CEPR2-mediated phosphorylation of NRT1.2 and PYLs balances growth and the ABA response in *Arabidopsis*. Under normal conditions, CEPR2 interacts with and phosphorylates PYLs, leading to degradation and the suppression of ABA signaling. Simultaneously, CEPR2 interacts with and phosphorylates NRT1.2, completely inhibiting ABA-import and stimulating NRT1.2 degradation. Thus, CEPR2 suppresses the ABA response by regulating ABA signaling and ABA import. Along with the environmental stimuli that result in ABA accumulation, ABA import and the ABA response are increased because ABA inhibits the phosphorylation of PYLs and NRT1.2, stabilizing PYLs and NRT1.2, and thus restoring the ABA binding ability of PYLs, as well as the ABA-importing activity of NRT1.2.